Palaeogeography, Palaeoclimatology, Palaeoecology 440 (2015) 712–724

Contents lists available at ScienceDirect

Palaeogeography, Palaeoclimatology, Palaeoecology

journal homepage: www.elsevier.com/locate/palaeo

Rare earth element and Sr–Nd isotope geochemistry of phosphatic rocks in Neoproterozoic Ediacaran Doushantuo Formation in Zhangcunping section from western Hubei Province, South China

Hong Xin [a], Shao-Yong Jiang [a,b,*], Jing-Hong Yang [a], He-Ping Wu [a], Dao-Hui Pi [b]

[a] State Key Laboratory for Mineral Deposits Research, Department of Earth Sciences, Nanjing University, Nanjing 210093, China
[b] State Key Laboratory of Geological Processes and Mineral Resources, Collaborative Innovation Center for Exploration of Strategic Mineral Resources, Faculty of Earth Resources, China University of Geosciences, Wuhan 430074, China

ARTICLE INFO

Article history:
Received 1 May 2015
Received in revised form 20 September 2015
Accepted 22 September 2015
Available online 30 September 2015

Keywords:
Phosphatic rocks
Rare earth elements
Sr–Nd isotopes
Neoproterozoic
Doushantuo Formation
South China

ABSTRACT

Phosphatic rocks are widely distributed in Neoproterozoic Ediacaran Doushantuo Formation in Yangtze Platform, South China. In this study, we examined samples from the Zhangcunping section in western Hubei Province with major element, rare earth element (REE) and Sr–Nd isotopic analyses on the phosphorites and the host dolostone rocks. We employed an acid-leaching method to separate the carbonate (acetic acid leachable) and phosphate (hydrochloric acid leachable) fractions in all the samples. The geochemical differences between the different fractions can be recognized based on the P_2O_5, REE contents and Sr–Nd isotopic characteristics. The carbonate fractions in the rocks display low total REE concentrations with seawater-like REE patterns, super-chondritic Y/Ho ratios, moderate negative Ce anomalies and positive Eu anomalies, indicating these carbonates have retained the signatures of paleo-seawater. On the contrary, the phosphate fractions display high total REE concentrations with hat-shaped REE patterns, generally lower Y/Ho ratios, weak negative Ce anomalies and positive Eu anomalies, which may have recorded the features of diagenetic fluids. Negative Ce anomalies and positive Eu anomalies displayed in the carbonate fractions of the studied samples may also indicate the anoxic environments of ocean basins in South China during the deposition of the Neoproterozoic Ediacaran Doushantuo Formation. A geochemical comparison between Lower Phosphorite Layer and Upper Phosphorite Layer indicates a greater degree of diagenesis occurred in the Lower Phosphorite Layer than the Upper Phosphorite Layer. The negative εNd(t) values of the samples suggest continental crustal sources for the REEs, and the lower values in the phosphorite samples (−6.9 to −6.0) than the dolostone samples (−5.5 to −3.8) may suggest different processes for them, and it is likely that the REEs in the phosphorites have been modified by diagenetic fluids with REE contributions of pore fluids derived from the clastic silicates in the strata which generally have lower εNd(t) values, whereas the dolostone took the REEs from the ambient seawater mainly.

1. Introduction

The Neoproterozoic Ediacaran Doushantuo Formation distributing in South China lasts from 635 Ma to 551 Ma, following the end-Neoproterozoic global ice age (Condon et al., 2005). As it contains both carbonate and silicic strata exhibiting different marine facies as well as abundant and well preserved multicellular fossils (e.g. Li et al., 1998; Xiao et al., 1998, 2002; Yin et al., 2007; Yuan et al., 2011; Zhu et al., 2003), the Doushantuo Formation provides a good target for the global research on the Neoproterozoic geology and the reconstruction of Ediacaran palaeoenvironment with different geochemical methods, which has become a focus study over the past decades (e.g. Ling et al., 2013; Liu et al., 2009; Zhou et al., 2005; Zhu et al., 2013a,b).

Phosphatic rocks are widely distributed in the Neoprotozoic Ediacaran Doushantuo Formation in South China, and generally dolostones occur as their host rocks. Paytan and McLaughlin (2007) proposed that marine phosphate sediments would prefer to grow at or below sediment–water interface with high biological productivity and low oxygen availability. Previous studies have shown that phosphates can incorporate affluent rare earth elements (REE) during their formation so that the REE contents, the REE patterns and the Ce and Eu anomalies of phosphates can provide valuable information of paleo-seawater (Kidder et al., 2003; McArthur and Walsh, 1984). However, more recent studies have shown that the REE characteristics of phosphates could be altered by diagenetic processes (e.g. Anderson et al., 2001; Chen et al., 2015;

* Corresponding author at: State Key Laboratory for Mineral Deposits Research (Nanjing) and State Key Laboratory of Geological Processes and Mineral Resources (Wuhan), China
E-mail addresses: shyjiang@cug.edu.cn, shyjiang@nju.edu.cn (S.-Y. Jiang).

http://dx.doi.org/10.1016/j.palaeo.2015.09.034
0031-0182/

German and Elderfield, 1990; Gnandi and Tobschall, 2003; Muscente et al., 2014; Shields and Stille, 2001; Shields and Webb, 2004; Webb and Kamber, 2000; Zhao et al., 2013).

In this study, we discussed the geochemical characteristics of the phosphatic rocks and their host dolostone rocks in the well-studied Zhangcunping section in western Hubei Province, South China, including the major element, REE and Nd–Sr isotopic analyses, in order to understand the paleo-seawater environment in Ediacaran Doushantuo epoch and the diagenetic processes during phosphogenesis.

2. Geological setting and studied section

The Ediacaran section located in western Hubei Province is one of the most important Neoproterozoic sections in the world, which are well exposed with abundant fossils and a long research history (Liu et al., 2009). Four members of the Ediacaran Doushantuo Formation are divided in the Yangtze Gorges area in Hubei Province, South China. In ascending stratigraphic order they are: (A) cap dolostone covering glacial diamictite of the Cryogenian Marinoan Formation; (B) black shale intercalated with muddy dolostone, containing abundant chert nodules or bandings; (C) medium-large-bedded dolostone with chert nodules or bandings and banded limestone upside; and (D) black shale with dolostone concretions (Liu et al., 2009; Sawaki et al., 2010; Wang et al., 1998; Zhou et al., 2005; Zhu et al., 2003).

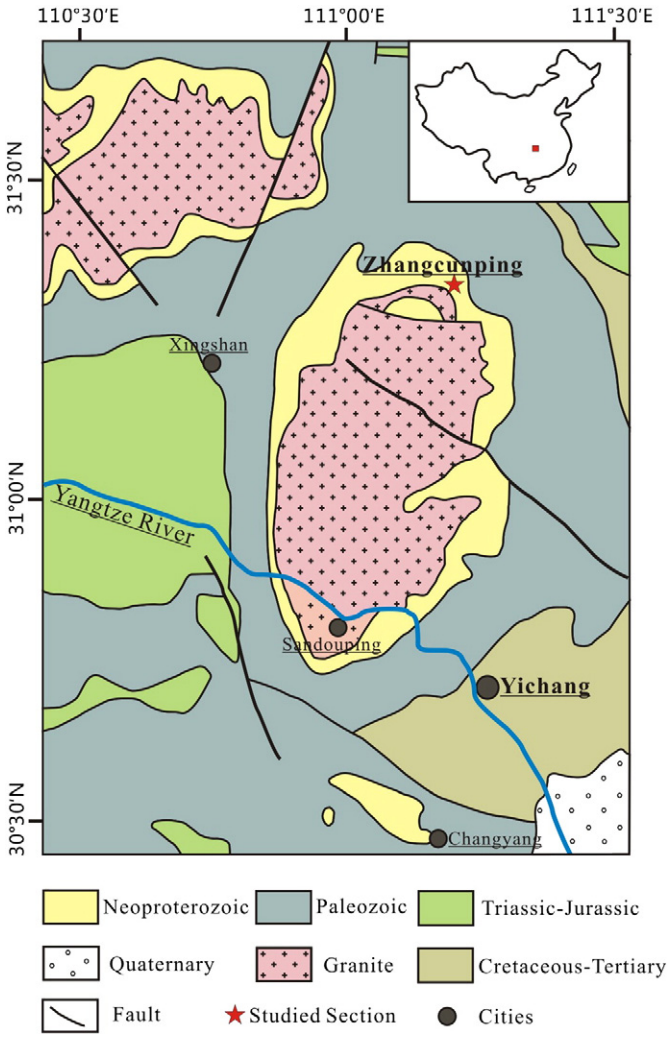

Fig. 1. Geological map of the Three Gorge area with location of the Zhangcunping section (After Zhu et al., 2013b).

The studied area is located at the northern limb of the Huangling anticline in the eastern Yangtze Gorges (Fig. 1). The oldest strata exposed in this area is the Archean Kongling group metamorphic rocks, which has an unconformable contact with the tillite of the Cryogenian Marinoan Formation (Zhou et al., 2005), and the Ediacaran Doushantuo Formation is well developed here (Fig. 1).

The Zhangcunping section of the Ediacaran Doushantuo Formation is situated at Wanjiagou phosphorite mine (111°11′29.11″E, 31°17′39.20″N), where the Doushantuo Formation is disconformable with the glacial diamictite of the Cryogenian Marinoan Formation downside. It consists of 10 layers and they are, in ascending stratigraphic order, (I) cap carbonate in 2 m; (II) black muddy shale with dolostone in 24 m; (III) thick banded collophanite layer in 4 m; (IV) dolostone with phosphatic bandings in 8 m; (V) medium-thick-bedded dolostone in 12 m; (VI) dolostone with thin-bedded shale in 3 m; (VII) dolostone with phosphatic bandings in 2 m; (VIII) dolostone with phosphatic nodules in 20 m; (IX) dolostone with black shale in 10 m; and (X) thick-bedded dolostone in 30 m (Fig. 2). Layer II to IX are the main compositions and represent the Member B of Ediacaran Doushantuo Formation in general (Fig. 2). There is an obvious discontinuity developed in the middle of the Section, and different phosphatic rocks develop both above and beneath this discontinuity. The Upper Phosphorite Layer manifests as phosphatic nodules and bandings while the Lower Phosphorite Layer as phosphatic bandings and thick banded collophanites.

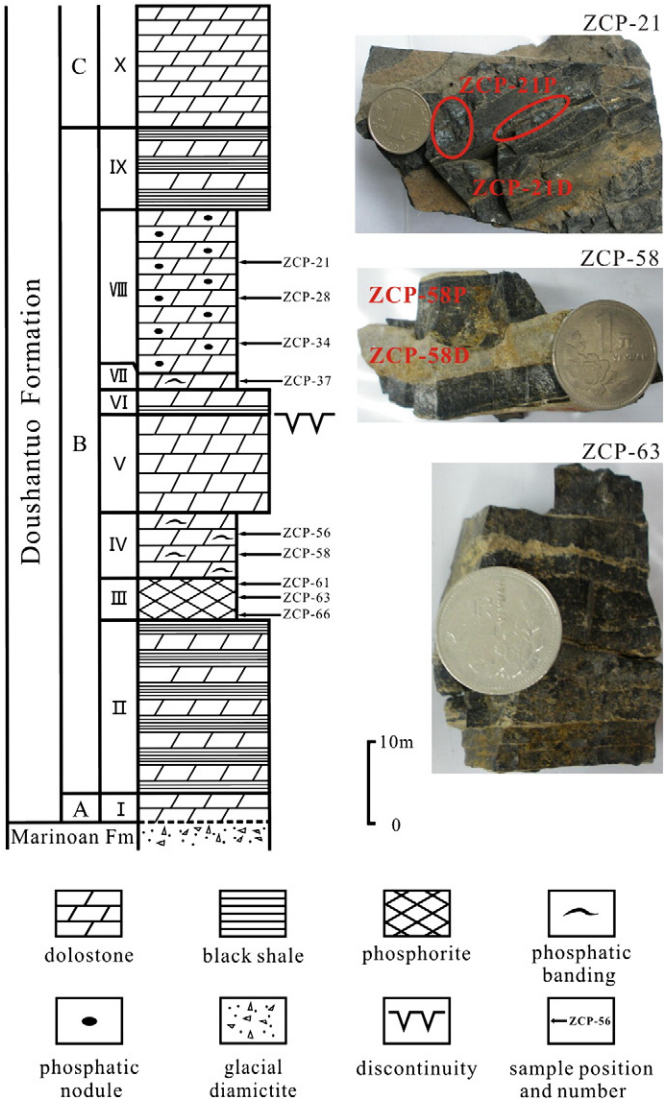

Fig. 2. Sketch stratigraphic column of the Zhangcunping section.

Condon et al. (2005) reported that the ages for the bottom and top Neoproterozoic Ediacaran Doushantuo Formation are 635.2 ± 0.6 Ma and 551.1 ± 0.7 Ma, respectively, based on the zircon U–Pb dating of volcanic tuff layers. A zircon U–Pb age of 632.5 ± 0.5 Ma for the bottom of the Member B of the Ediacaran Doushantuo Formation was also reported by Condon et al. (2005). A Re–Os age of 591.1 ± 5.3 Ma for the Ediacaran Doushantuo Formation black shales was reported by Zhu et al. (2013a). Liu et al. (2009) reported a zircon U–Pb age of 614.0 ± 7.6 Ma below the erosional disconformity at our studied area, just between layer IV and layer V (Fig. 2). As there is no other report for the exact age of the phosphorite formation, we suggest that 614 Ma can be used as the lower limit age of the phosphorite.

3. Samples and analytical methods

In this study, nine phosphatic rock samples were selected from the Zhangcunping section. Among these samples there are three phosphatic nodule samples and one phosphatic banding sample from Upper Phosphorite Layer, while two phosphatic banding samples and three thick banded collophanite samples from Lower Phosphorite Layer (Fig. 2). We cut the phosphorite ore and the host-dolostone into two parts in the same rock sample as two sub-samples and named them as ZCP-21P and ZCP-21D, respectively, for example for the Sample ZCP-21. All fifteen samples were crushed to powder less than 200-mesh in an agate mill.

Generally speaking, all the studied samples consist of three components, i.e., carbonate fraction, phosphate fraction and silicate fraction. Most of the silicate materials in these marine sediments may have been derived from detrital components being transported by river water from the continents, and only the carbonate and phosphate materials in the rocks are of syn-sedimentary origin and can record the geochemical characteristics of palaeo-seawater and/or porewaters. Therefore, in this study we applied the acid leaching technique to dissolve only the carbonate and phosphate materials in the bulk samples for REE and isotopic analysis respectively. This technique has been applied by many previous researchers, for example, Shields and Stille (2001) used hydrochloric acid leaching method for isotopic and REE study of Cambrian phosphorites, and so did Jiang et al. (2007) and Zhu et al. (2014) for similar rocks. Besides, Guo et al. (2007) used hydrochloric acid leaching to remove calcium phosphate minerals for chemostratigraphy study for organosedimentary metal enrichment and silicification in the early Cambrian.

3.1. Major element analysis

In order to get rid of the influence of the silicate materials in the samples, about 20 mg of each sample powders was treated with 6 N hydrochloric acid, placed in an ultrasonic bath for half an hour and then reacted at room temperature for at least 12 h. After dissolution, the solutions were centrifuged and the supernatants of carbonate and phosphate fractions were separated, attenuated and calibrated, meanwhile the residues of silicate fractions were abandoned. Major elements were analyzed by an ICP-AES (JY38S), with the analytical precision better than 2% RSD (relative standard deviation).

3.2. Rare earth element and yttrium analysis

About 100 mg was weighed and dissolved using a step leaching method to separate two fractions in each sample, first in 1 N acetic acid to dissolve the carbonate fractions (Jiang et al., 2007; Ling et al., 2013; Nothdurft et al., 2004) and then in 1 N hydrochloric acid to release the phosphate fractions in the same sample (Guo et al., 2007; Jiang et al., 2007; Shields and Stille, 2001; Zhu et al., 2014). After first dissolution in 1 N acetic acid, the samples were centrifuged and the supernatants were transferred into clean Teflon beakers. Then the residues were dissolved in 1 N hydrochloric acid on a hotplate at about 120 °C for at least 12 h to further dissolve the phosphate fractions. Again after this dissolution step, the solutions were centrifuged and the supernatants were transferred. The supernatants of both fractions were evaporated to near dryness on a hotplate at about 120 °C, and then 1 mL concentrated nitric acid was added into the beakers and dried twice to remove the acetic acid or hydrochloric acid in the samples. Then the nearly dried samples were dissolved in 3% nitric acid and calibrated to 10 mL to be analyzed while doped by 0.2 mL 500 ppb Rh as internal standard (Jiang et al., 2007; Zhu et al., 2014). Rare earth elements were analyzed by an ICP-MS (Aurora M90, Bruker) and determined by linear regression to laboratory standards, while the analytical precision is better than 10% RSD.

Ce, Eu and Pr anomalies in both the carbonate and phosphate fractions were calculated using the equations $Ce/Ce^* = 3Ce_N/(2La_N + Nd_N)$, $Eu/Eu^* = 2Eu_N/(Sm_N + Gd_N)$, and $Pr/Pr^* = 2Pr_N/(Ce_N + Nd_N)$ (Bau and Dulski, 1996; De Baar et al., 1991), where N refers to the normalization of concentrations against the post-Archen Australian shale (PAAS) standard (McLennan, 1989).

3.3. Sr–Nd isotope analysis

Eleven of fifteen samples were analyzed with Sr–Nd isotopes and the same dissolution method was used as the rare earth element analysis. After the separation of all supernatants, they were dried up and added with 1 mL 4 N hydrochloric acid. After the ultrasonic bath for half an hour, the supernatants were centrifuged again and the Sr and Nd were separated with the chromatographic procedure described by Pu et al. (2005). Sr and Nd isotopic compositions were measured on an MC-ICP-MS (Neptune-Plus, Thermo Fisher Scientific) and determined with the method of internal standardization for mass bias correction via exponential law (Yang, 2009). The mass fractionation on $^{87}Sr/^{86}Sr$ and $^{143}Nd/^{144}Nd$ ratios was corrected based on natural $^{86}Sr/^{88}Sr = 0.1194$ and $^{146}Nd/^{144}Nd = 0.7219$. The Sr standard NIST 987 and Nd standard SPEX were analyzed repeatedly with $^{87}Sr/^{86}Sr$ of 0.710281 ± 0.000012 (2σ, n = 7) and $^{143}Nd/^{144}Nd$ of 0.511665 ± 0.000012 (2 σ, n = 6), respectively.

All the analyses were carried out at State Key Laboratory for Mineral Deposits Research in Nanjing University.

4. Results

4.1. Major elements

Major element concentrations are listed in Table 1. Since we used a hydrochloric acid leaching method, no silicate should be dissolved in the samples, hence no SiO_2 components were shown. Meanwhile CO_2 might escape during the acid leaching process, the total major element concentrations in the bulk rocks are therefore less than 100 wt.% depending on the relative contents of the carbonate-phosphate and the silicate fractions in the samples.

As shown in Table 1, samples from the Upper Phosphorite Layer have much lower total major element concentrations (6.26–47.81 wt.%) than the samples from the Lower Phosphorite Layer (54.51–85.51 wt.%), which indicate that the Upper Phosphorite Layer samples contain higher amounts of silicate components. CaO and P_2O_5 are the major compositions in most phosphorite sub-samples, ranging from 3.88 to 51.25 wt.% and 1.76 to 32.15 wt.% respectively, with P_2O_5/CaO ratios of 0.24–0.71. CaO and MgO are the major compositions in dolostone sub-samples, ranging from 6.75 to 34.71 wt.% and 0.79 to 22.61 wt.%, respectively, with MgO/CaO ratios of 0.12–0.75. The samples from the Lower Phosphorite Layer generally show higher P_2O_5 concentrations and higher P_2O_5/CaO ratios than the ones from the Upper Phosphorite Layer. Other oxide concentrations in most samples are less than 1 wt.%.

4.2. Rare earth elements and yttrium

REE analytical results of both the phosphate and carbonate fractions are listed in Table 2. The phosphate fractions show a total REE (ΣREE)

Table 1
Major element concentrations of the bulk rock samples from the Zhangcunping section.

Sample	ZCP-21D	ZCP-21P	ZCP-28D	ZCP-28P	ZCP-34D	ZCP-34P	ZCP-37D	ZCP-37P	ZCP-56D	ZCP-56P	ZCP-58D	ZCP-58P	ZCP-61	ZCP-63	ZCP-66
TiO_2	0.00	0.00	0.00	0.00	0.01	0.00	0.00	0.01	0.00	0.01	0.00	0.00	0.01	0.01	0.01
Al_2O_3	0.36	0.12	0.34	0.08	0.13	0.05	0.16	1.10	0.39	0.68	0.24	0.31	0.62	0.73	0.63
FeO	0.77	0.16	0.64	0.11	0.11	0.08	0.38	1.70	0.21	0.22	0.86	0.18	0.26	0.45	0.21
MnO	0.02	0.00	0.01	0.00	0.02	0.00	0.01	0.00	0.04	0.01	0.06	0.01	0.01	0.01	0.01
MgO	13.69	0.39	13.03	0.30	17.93	2.34	0.79	0.19	20.72	0.37	22.61	0.31	0.27	0.39	0.32
CaO	24.09	5.71	27.85	3.88	25.52	7.35	6.75	28.24	34.71	50.26	30.13	48.77	51.25	44.44	44.92
Na_2O	0.06	0.01	0.11	0.01	0.06	0.02	0.03	0.21	0.06	0.72	0.03	0.64	0.78	0.88	0.81
K_2O	0.21	0.04	0.26	0.04	0.04	0.03	0.08	0.57	0.02	0.55	0.02	0.04	0.16	0.63	0.58
P_2O_5	4.03	2.25	5.56	1.83	0.42	1.76	3.47	14.29	3.80	31.32	0.55	28.79	32.15	31.71	31.55
Total	43.24	8.68	47.81	6.26	44.23	11.64	11.66	46.32	59.96	84.14	54.51	79.04	85.51	79.23	79.03
MgO/CaO	0.57	0.07	0.47	0.08	0.70	0.32	0.12	0.01	0.60	0.01	0.75	0.01	0.01	0.01	0.01
P_2O_5/CaO	0.17	0.39	0.20	0.47	0.02	0.24	0.51	0.51	0.11	0.62	0.02	0.59	0.63	0.71	0.70

concentration range from 2.17 to 496.7 ppm, with low Y/Ho ratios (25.50 to 46.07), negative Ce anomalies ($Ce/Ce^* = 0.62$ to 0.96) and positive Eu anomalies ($Eu/Eu^* = 1.01$ to 1.32), respectively. The phosphate fractions in the phosphorite sub-samples from the Lower Phosphorite Layer show higher ΣREE concentrations, lower Y/Ho ratios, higher Ce/Ce^* and higher Eu/Eu^* values than the ones from the Upper

Table 2
Contents of REE and Ba in the phosphate and carbonate fractions of the rock samples. ($Ce/Ce^* = 3Ce_N/(2La_N + Nd_N)$, $Eu/Eu^* = 2Eu_N/(Sm_N + Gd_N)$, and $Pr/Pr^* = 2Pr_N/(Ce_N + Nd_N)$ (Bau and Dulski, 1996; De Baar et al., 1991), where N refers to the normalization of concentrations against the post-Archen Australian shale (PAAS) standard (McLennan, 1989)).

Sample	ZCP-21D	ZCP-21P	ZCP-28D	ZCP-28P	ZCP-34D	ZCP-34P	ZCP-37D	ZCP-37P	ZCP-56D	ZCP-56P	ZCP-58D	ZCP-58P	ZCP-61	ZCP-63	ZCP-66
Phosphate fractions (ppm)															
La	10.14	3.26	16.62	3.51	1.57	4.66	13.35	94.73	3.52	19.36	0.45	20.94	17.45	14.62	20.24
Ce	17.99	5.49	26.68	5.63	2.72	7.57	24.32	170.05	5.62	38.73	0.84	29.58	36.12	30.31	40.20
Pr	3.20	0.97	5.04	1.06	0.56	1.56	4.63	30.57	0.86	4.30	0.10	3.21	3.79	3.30	4.50
Nd	13.91	4.33	21.79	4.73	2.40	7.05	20.74	125.66	3.39	18.24	0.40	11.15	17.12	14.18	18.86
Sm	3.04	0.98	4.57	1.06	0.47	1.53	4.38	22.47	0.62	3.24	0.08	1.63	2.96	2.33	3.52
Eu	0.73	0.27	1.04	0.26	0.10	0.43	1.05	5.09	0.13	0.85	0.02	0.40	0.74	0.64	0.91
Gd	3.06	1.10	4.44	1.11	0.46	1.51	3.91	19.90	0.59	2.91	0.08	1.69	2.75	2.18	3.17
Tb	0.47	0.17	0.67	0.17	0.07	0.22	0.58	2.77	0.09	0.40	0.01	0.21	0.37	0.29	0.44
Dy	2.64	0.99	3.66	0.99	0.37	1.19	2.90	13.20	0.45	1.92	0.07	0.95	1.84	1.36	2.06
Ho	0.52	0.20	0.72	0.20	0.07	0.22	0.51	2.23	0.08	0.33	0.01	0.17	0.34	0.25	0.35
Er	1.37	0.52	1.94	0.52	0.18	0.53	1.23	6.12	0.22	0.83	0.04	0.46	0.93	0.66	0.89
Tm	0.16	0.06	0.23	0.06	0.02	0.05	0.12	0.62	0.03	0.08	0.01	0.05	0.11	0.07	0.09
Yb	0.80	0.29	1.20	0.29	0.10	0.24	0.58	2.93	0.14	0.42	0.04	0.27	0.61	0.38	0.45
Lu	0.10	0.04	0.16	0.04	0.01	0.03	0.07	0.36	0.02	0.05	0.01	0.04	0.08	0.05	0.06
Y	19.87	8.18	29.70	7.49	2.47	7.41	15.96	102.88	2.53	9.03	0.50	5.61	9.59	6.60	8.97
ΣREE	58.14	18.66	88.75	19.63	9.11	26.79	78.37	496.70	15.74	91.68	2.17	70.75	85.23	70.63	95.75
Y/Ho	38.36	41.94	41.24	38.14	35.22	34.39	31.45	46.07	31.06	27.36	35.03	32.75	28.04	26.86	25.50
Ce/Ce^*	0.71	0.69	0.66	0.65	0.66	0.62	0.69	0.73	0.74	0.93	0.89	0.78	0.95	0.96	0.93
Eu/Eu^*	1.13	1.19	1.08	1.14	1.05	1.32	1.20	1.13	1.05	1.30	1.01	1.12	1.22	1.32	1.29
Pr/Pr^*	1.12	1.10	1.15	1.12	1.20	1.15	1.12	1.17	1.12	0.94	1.01	1.03	0.88	0.92	0.95
La_N/Sm_N	0.48	0.48	0.53	0.48	0.48	0.44	0.44	0.61	0.83	0.87	0.78	1.86	0.86	0.91	0.83
Dy_N/Sm_N	1.03	1.19	0.95	1.11	0.94	0.92	0.78	0.70	0.85	0.70	1.02	0.69	0.74	0.69	0.69
Ba	8.91	29.77	22.90	14.61	4.75	287.58	44.62	114.18	3.51	360.34	5.66	202.46	227.07	311.46	316.30
Ba/Nd	0.64	6.88	1.05	3.09	1.98	40.80	2.15	0.91	1.03	19.75	14.12	18.16	13.26	21.96	16.77
Carbonate fractions (ppb)															
La	460.8	27.90	199.7	24.98	684.7	58.23	310.8	126.5	376.56	7.29	39.68	7.21	25.52	5.03	11.40
Ce	622.7	14.80	222.9	6.67	896.1	40.49	487.2	147.70	491.3	9.97	49.92	10.27	30.25	7.70	9.27
Pr	101.7	11.52	49.19	11.11	160.9	17.97	93.13	35.77	62.91	3.48	11.64	2.91	9.94	5.86	7.15
Nd	520.6	64.17	279.2	60.99	723.2	101.2	457.5	194.45	256.5	17.21	50.37	13.34	45.78	26.68	32.76
Sm	103.5	13.75	57.49	13.24	137.8	20.96	87.51	35.29	49.60	5.06	10.96	3.88	9.56	6.15	7.79
Eu	26.14	18.03	15.88	12.61	35.05	32.68	25.37	17.13	11.97	37.97	7.63	16.21	28.18	22.59	41.21
Gd	109.4	16.50	63.23	14.27	134.8	22.20	83.41	35.77	56.16	4.50	11.04	3.53	9.33	5.70	7.21
Tb	18.13	2.37	9.67	2.05	23.75	3.23	11.69	4.83	9.83	0.55	1.85	0.42	1.26	0.73	0.93
Dy	109.7	15.04	59.60	13.27	150.7	20.50	61.33	26.76	70.65	4.46	13.07	3.84	7.98	5.39	6.25
Ho	23.82	3.00	13.54	2.58	32.20	4.16	10.86	5.00	16.81	1.05	2.65	0.81	1.20	0.72	0.80
Er	74.86	10.49	41.28	9.38	100.5	14.37	30.68	14.90	60.86	3.68	11.23	3.36	5.45	4.13	4.27
Tm	10.32	1.17	5.12	1.04	14.10	1.64	3.02	1.53	9.84	0.35	1.79	0.35	0.62	0.44	0.44
Yb	64.71	5.00	28.58	4.32	88.65	9.01	14.19	6.13	69.87	1.17	11.47	1.11	1.88	1.00	1.10
Lu	11.50	1.08	5.49	0.97	14.34	1.81	2.24	1.21	12.91	0.45	2.38	0.40	0.58	0.47	0.49
Y	1067.4	115.4	552.0	94.66	1294	152.9	435.1	178.2	836.4	26.61	76.22	27.85	37.16	24.43	23.25
ΣREE	2257.9	204.8	1050.9	177.5	3196.9	348.4	1678.9	653.0	1555.7	97.18	225.7	67.62	177.5	92.59	131.1
Y/Ho	44.81	38.41	40.78	36.67	40.18	36.76	40.06	35.66	49.74	25.43	28.75	34.24	31.03	33.78	29.03
Ce/Ce^*	0.59	0.16	0.44	0.08	0.59	0.25	0.61	0.45	0.67	0.42	0.52	0.50	0.42	0.27	0.22
Eu/Eu^*	1.15	5.55	1.23	4.28	1.21	7.09	1.40	2.26	1.06	37.46	3.25	20.60	14.02	17.96	25.86
Pr/Pr^*	0.98	1.23	0.99	1.31	1.10	1.14	1.06	1.05	1.02	1.22	1.23	1.24	1.28	1.47	1.46
La_N/Sm_N	0.65	0.29	0.50	0.27	0.72	0.40	0.52	0.52	1.10	0.21	0.53	0.27	0.39	0.12	0.21
Dy_N/Sm_N	1.26	1.30	1.23	1.19	1.30	1.16	0.83	0.90	1.69	1.05	1.41	1.17	0.99	1.04	0.95
Ba	9556	381506	114471	238639	136941	593356	199287	230980	6084	557528	114042	284852	411050	355080	633324
Ba/Nd	18.36	594.5	41.00	391.3	18.93	586.6	43.55	118.8	23.72	3240	226.4	2136	897.8	1331	1933

Phosphorite Layer. The phosphate fractions in the dolostone sub-samples from the Lower Phosphorite Layer show lower ΣREE concentrations, lower Y/Ho ratios, lower Ce/Ce* and higher Eu/Eu* values than the ones from the Upper Phosphorite Layer.

In the carbonate fractions leached by acetic acid, the total REE concentrations range from 0.0667 to 3.197 ppm, with Y/Ho ratios varying from 25.43 to 49.74. Negative Ce anomalies (Ce/Ce* = 0.08 to 0.67) and positive Eu anomalies (Eu/Eu* = 1.06 to 37.46) are also shown in all samples. The carbonate fractions in the phosphorite sub-samples show lower ΣREE concentrations, lower Y/Ho ratios, lower Ce/Ce* values and higher Eu/Eu* values than those in the dolostone sub-samples. The carbonate fractions in the phosphorite sub-samples from the Lower Phosphorite Layer show lower ΣREE concentrations, lower Y/Ho ratios, higher Ce/Ce* and higher Eu/Eu* values than the ones from the Upper Phosphorite Layer. The carbonate fractions in the dolostone sub-samples from the Lower Phosphorite Layer show lower ΣREE concentrations than the ones from the Upper Phosphorite Layer.

4.3. Sr–Nd isotopes

Sr and Nd isotopic ratios are listed in Table 3. As extremely low Nd concentrations in the carbonate fractions, the Nd isotopic ratios have not been analyzed in these parts as well as in one dolostone sub-sample. The $^{143}Nd/^{144}Nd$ ratios of the phosphate fractions range from 0.511889 to 0.512127 and the εNd(t) values vary from −6.9 to −3.8 when calculated at 614 Ma. The phosphorite sub-samples show a lower εNd(t) variation (−6.9 to −6.0) than the dolostone sub-samples (−5.5 to −3.8).

The $^{87}Sr/^{86}Sr$ ratios of the phosphate and carbonate fractions in the samples vary from 0.709942 to 0.716799 and 0.708513 to 0.718692, respectively. The initial $^{87}Sr/^{86}Sr$ ratios calculated at 614 Ma range from 0.709876 to 0.716797 and 0.708504 to 0.718641, respectively. Generally speaking, the dolostone sub-samples display lower initial $^{87}Sr/^{86}Sr$ ratios than the phosphorite sub-samples and the samples from the Upper Phosphorite Layer display lower initial $^{87}Sr/^{86}Sr$ ratios than the Lower Phosphorite Layer.

5. Discussion

5.1. REE patterns

It is well known that phosphatic sediments contain larger amount of REE and yttrium (Y) compared to the other sedimentary rocks due to the substitution of REE^{3+} and Y^{3+} for Ca^{2+} in apatite (Jarvis et al., 1994; Kidder et al., 2003; Trappe, 1998) as well as the adsorption/desorption processes of REEs by mineral particulates (Chen et al., 2015; Shields and Webb, 2004; Webb and Kamber, 2000; Zhao et al., 2013). As a result, the REEs of the phosphatic rocks can be used to indicate the depositional and/or diagenetic environments as they may record the REE characteristics of the seawater in equilibrium with the phosphorites at the time of their formation (Zhu et al., 2014). However, different REE suppliers (McArthur and Walsh, 1984) and diagenetic overprinting (German and Elderfield, 1990; Reynard et al., 1999; Shields and Stille, 2001) may result to a wide variety of the shale-normalized REE patterns in modern and ancient phosphorite deposits (e.g. Jiang et al., 2007; Pi et al., 2013; Trappe, 1998; Zhu et al., 2014), including seawater-like pattern and hat-shaped pattern (Reynard et al., 1999).

The so-called hat-shaped pattern is characteristic of MREE-enrichment and HREE-depletion, which occurs very often in many phosphate sediments. For example, Ilyin (1998) proposed that the so-called "old phosphorite" REE patterns exist in most phosphorites older than Mesozoic with HREE depletion and remarkable negative Ce anomaly, and he suggested that these patterns could record the seawater geochemical characteristics when the phosphorite formed. However, the shale-normalized REE patterns of seawater have hardly changed during Phanerozoic in light of the research of Shields and Webb (2004), which are characterized by negative Ce anomalies and HREE enrichment. Jiang et al. (2007) and Zhu et al. (2014) reported the seawater-like REE patterns in the early-Cambrian phosphatic nodules, strongly supporting the similar patterns existing both in ancient and modern oceans. More recent researches have shown the diagenetic evidences to interpret the hat-shaped REE pattern alteration of phosphatic rocks (e.g. Anderson et al., 2001; Chen et al., 2015; Gnandi and Tobschall, 2003; Muscente et al., 2014; Webb and Kamber, 2000; Zhao et al., 2013).

In this study, mainly two types of REE patterns are displayed as shown in Figs. 3 and 4. One type is the hat-shaped REE pattern displayed in the phosphate fractions of almost all samples (Fig. 3). The typical hat-shaped REE patterns are displayed in the samples from Upper Phosphorite Layer (Fig. 3a–d), with Ce/Ce* values ranging from 0.62 to 0.73. On the contrary, the samples from the Lower Phosphorite Layer display a less typical hat-shaped REE pattern with more LREE-enrichment compared to the typical ones and weaker negative Ce anomalies (Fig. 3e–h), with Ce/Ce* values varying from 0.74 to 0.96. All samples show the same REE patterns in both the phosphorite ore and host dolostone sub-samples (Fig. 3a–f). The typical hat-shaped REE patterns were also reported in Neoproterozoic phosphatic rocks (Felitsyn and Morad, 2002) as well as in early-Cambrian phosphatic rocks (Jiang et al., 2007; Pi et al., 2013; Zhu et al., 2014). Meanwhile the less typical hat-shaped REE patterns were also reported by Pi et al. (2013) as one of the four groups of REE patterns as well as by Ilyin (1998) and Mazumdar et al. (1999) from the Precambrian–Cambrian phosphorites, reflecting diagenetic modifications (McArthur and Walsh, 1984). It is also a common phenomenon in modern marine phosphate sediments (Rasmussen et al., 1998).

The other type is the seawater-like REE pattern displayed in the carbonate fractions of most samples. It is characteristic of HREE-enrichment and negative Ce anomalies with respect to La and Pr (Bau

Table 3
Sr–Nd isotopic compositions of the phosphate and carbonate fractions in the rock samples.

Sample	Phosphate fractions				Phosphate fractions				Carbonate fractions			
	$^{143}Nd/^{144}Nd$	2σ (×10⁻⁶)	$^{147}Sm^{144}/Nd$	εNd(t)	$^{87}Sr/^{86}Sr$	2σ (×10⁻⁶)	$^{87}Rb^{86}/Sr$	$(^{87}Sr/^{86}Sr)_i$	$^{87}Sr/^{86}Sr$	2σ (×10⁻⁶)	$^{87}Rb^{86}/Sr$	$(^{87}Sr/^{86}Sr)_i$
ZCP-21D	0.512092	12	0.132	−5.5	0.710126	3	0.019	0.709958	0.709062	3	0.003	0.709035
ZCP-21P	0.512088	8	0.137	−6.0	0.712149	2	0.009	0.712068	0.712678	5	0.055	0.712188
ZCP-34D	0.512127	5	0.119	−3.8	0.709942	1	0.008	0.709876	0.708513	9	0.001	0.708504
ZCP-34P	0.512037	15	0.131	−6.5	0.715207	9	0.005	0.715166	0.711962	9	0.012	0.711851
ZCP-37D	0.512042	3	0.108	−4.6	0.714132	6	0.035	0.713818	0.713491	2	0.045	0.713092
ZCP-37P	0.512031	8	0.128	−6.4	0.715083	2	0.041	0.714720	0.713522	2	0.035	0.713213
ZCP-58D	–	–	–	–	0.713215	3	0.002	0.713197	0.712894	4	0.000	0.712892
ZCP-58P	0.511892	7	0.088	−6.0	0.716799	4	0.000	0.716797	0.718027	1	0.001	0.718018
ZCP-61	0.511914	12	0.104	−6.8	0.716082	2	0.006	0.716029	0.718692	7	0.006	0.718641
ZCP-63	0.511889	9	0.099	−6.9	0.715915	7	0.015	0.715780	0.718207	11	0.006	0.718156
ZCP-66	0.511976	7	0.113	−6.3	0.714512	7	0.015	0.714375	0.717000	10	0.015	0.716865

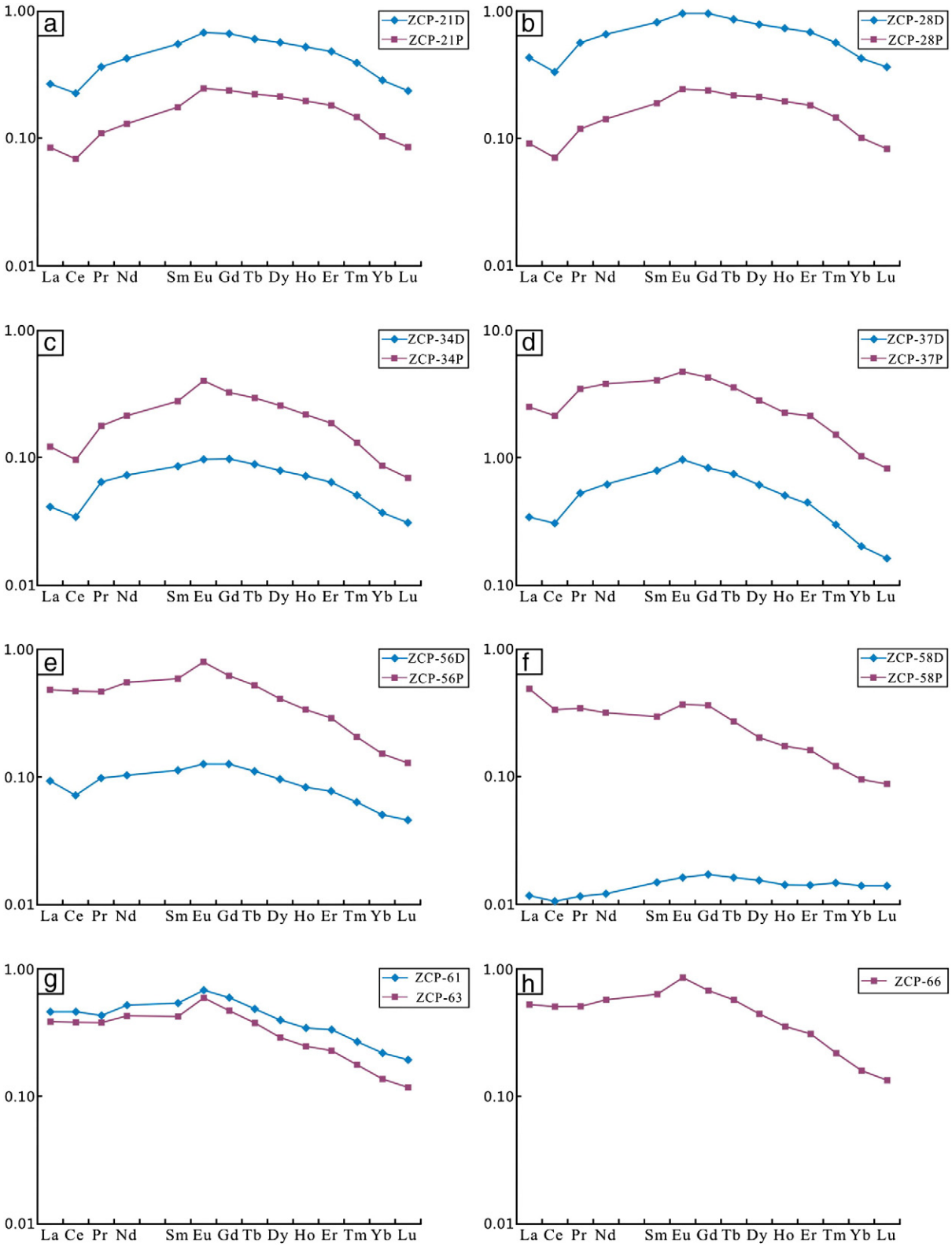

Fig. 3. Shale-normalized REE patterns of the phosphate fractions of the Zhangcunping section samples.

and Dulski, 1996) (Fig. 4). The typical seawater-like REE patterns are displayed in three of the four samples from the Upper Phosphorite Layer (Fig. 4a–c) with Ce/Ce* values ranging from 0.08 to 0.59, in which the phosphorite sub-samples displaying stronger negative Ce anomalies. On the contrary, the samples from the Lower Phosphorite Layer display a less typical seawater-like REE patterns with HREE-fluctuation, especially in the phosphorite sub-samples (Fig. 4e–h), with Ce/Ce* values ranging from 0.22 to 0.50. The remarkable positive Eu anomalies are displayed in all phosphorite sub-samples with Eu/Eu* values ranging from 4.28 to 37.46, while higher in the Lower

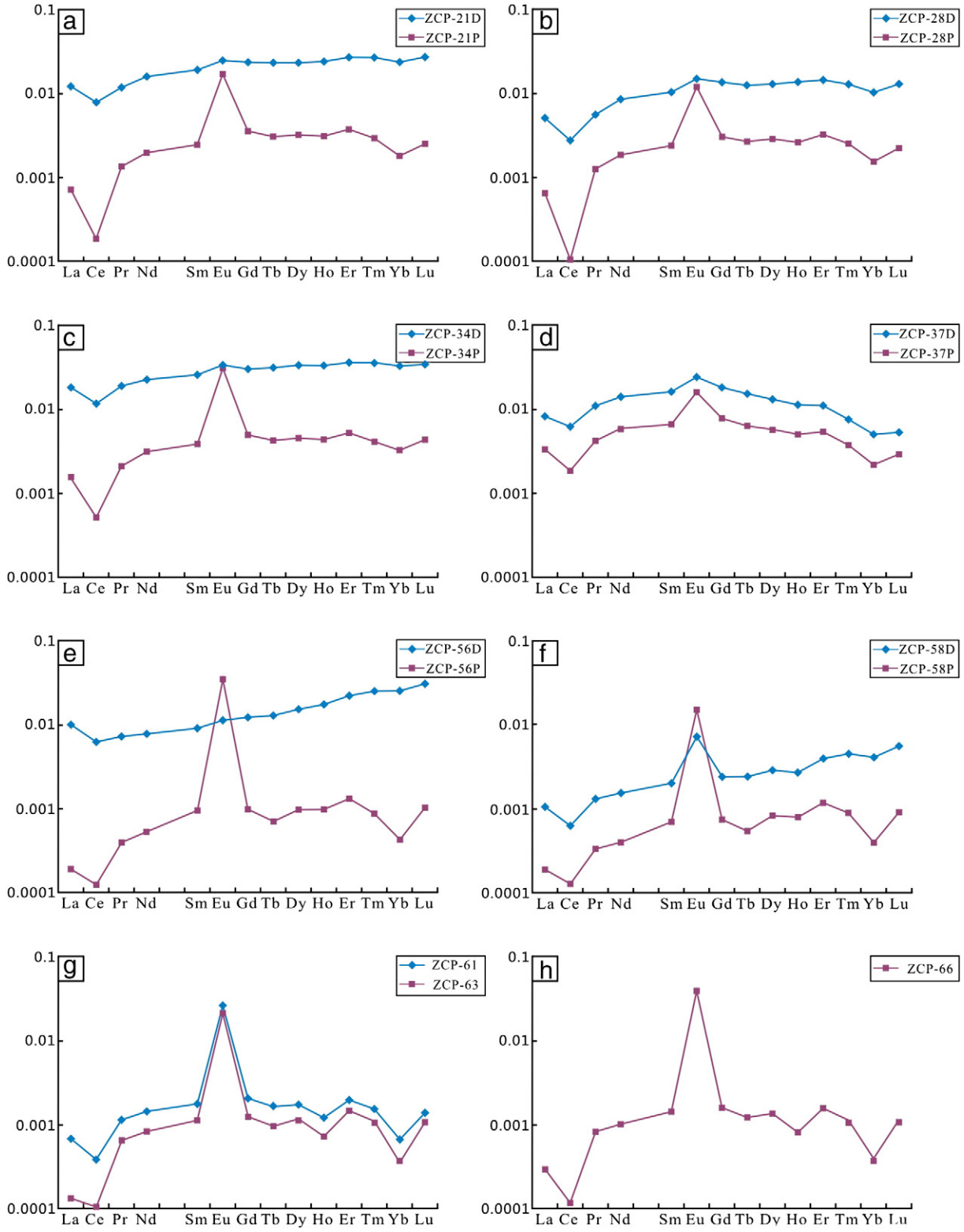

Fig. 4. Shale-normalized REE patterns of the carbonate fractions of the Zhangcunping section samples.

Phosphorite Layer than the Upper Phosphorite Layer. The typical seawater-like REE patterns were also reported in the core of early-Cambrian phosphatic nodule samples by Jiang et al. (2007) and Zhu et al. (2014), suggesting that primary seawater REE distribution patterns were similar to the modern seawater pattern. However the HREE-fluctuation REE patterns may reflect the greater diagenetic alteration effects in the Lower Phosphorite Layer.

Shields and Stille (2001) proposed that diagenetic processes can result in higher REE contents, preferential enrichment of MREE in phosphorites, and decrease in Ce anomalies. Compared to the seawater-like REE patterns displayed in the carbonate fractions of each bulk sample, the phosphate fractions with hat-shaped REE patterns characterized by MREE-enrichment may result from both substitution of REEs into apatite lattice structure (e.g. Kidder et al., 2003; Morad and Felitsyn, 2001;

Reynard et al., 1999; Wright et al., 1987) and particulate adsorption/desorption processes (e.g. Chen et al., 2015; Nothdurft et al., 2004; Picard et al., 2002; Shields and Webb, 2004; Webb and Kamber, 2000; Zhao et al., 2013). As a result, the carbonate fractions of the samples, especially the Upper Phosphorite Layer ones, should have the potential to contain the REE information of ambient seawater during sedimentation (Nothdurft et al., 2004; Shields and Webb, 2004; Webb and Kamber, 2000) in the meanwhile the phosphate fractions may contain the REE information of diagenetic processes due to diagenetic alteration (Chen et al., 2015; Morad and Felitsyn, 2001; Shields and Stille, 2001; Zhao et al., 2013).

The REE characteristics show significant difference between the Lower and Upper Phosphorite Layers. Both the LREE-enrichment in phosphate fractions and the HREE-fluctuation in carbonate fractions show the greater diagenetic alteration during phosphogenesis. Besides, the samples from the Lower Phosphorite Layer display higher ΣREE concentrations in the bulk rocks. The higher P_2O_5 concentrations indicating more apatite contents in the Lower Phosphorite Layer may be responsible for the higher ΣREE concentrations, and the ΣREE concentrations also show positive linear correlation with the contents of P_2O_5 wt.% in both the Upper and Lower Phosphorite Layers (Fig. 5). Due to more exposure time and larger surface/mass ratios, the compact banded phosphorite contains more REEs than the phosphatic nodules surrounded by dolostones.

Phosphatic rocks are known to grow at or below sediment–water interface (Morad and Al-Aasm, 1994; Paytan and McLaughlin, 2007). The seawater signatures in the pore water can be preserved due to the exchange between seawater and pore water in porous sediments at the beginning of the phosphate growth. The different REE patterns in different fractions may record the pore water REE geochemical changes during the diagenetic processes. Seawater REE characteristics were mainly protected in the carbonate fractions and the diagenetic fluids REE information was recorded in the phosphate fractions.

5.2. Ce anomaly

Ce anomaly in the seawater is mainly controlled by redox conditions so that it can be used as a tracer to reveal the redox conditions in the geological past (e.g. German and Elderfield, 1990; Jiang et al., 2007; Wright et al., 1987; Zhu et al., 2014). Moreover, microbial activity, pH value, water depth and the age of seawater can also influence Ce anomaly to some extent (German and Elderfield, 1990; Moffett, 1990).

In our study, negative Ce anomalies are shown in both the phosphate and carbonate fractions, with Ce/Ce^* values ranging from 0.62 to 0.96 and 0.08 to 0.67 respectively, indicating anoxic conditions. However, negative Ce anomalies could be overstated by high La concentrations so that Pr/Pr^* can be used to assess the degree of La effect (Bau and Dulski, 1996). As shown in Fig. 6a, most carbonate fractions of the samples and the phosphate fractions of samples from the Upper Phosphorite Layer are plotted in area IIIb, which means that these Ce anomalies are real values without exaggeration of La concentrations (Bau and Dulski, 1996). In addition, Morad and Felitsyn (2001) suggested that natural Ce anomalies should be get rid of the influence of artificial calculations under the condition of $La_N/Sm_N > 0.35$ and rare relation between La_N/Sm_N ratios and Ce/Ce^* values. As shown in Fig. 6b, La_N/Sm_N ratios of the phosphate fractions range from 0.44 to 1.86 with a strong positive correlation to Ce/Ce^* values ($R^2 = 0.84$), in which the dolostone sub-samples displaying weak correlation between the two parameters ($R^2 = 0.44$). The ones of carbonate fractions range from 0.12 to 1.10 with a weak positive correlation to Ce/Ce^* values ($R^2 = 0.54$), in which the dolostone sub-samples display higher La_N/Sm_N ratios. Combining the two parameters, negative Ce anomalies can only be identified to keep the paleo-seawater signatures and paleo-redox conditions in the carbonate fractions of the samples, especially in the dolostone sub-samples.

As Ce anomalies are changeable during diagenetic processes, Shields and Stille (2001) suggested that diagenetic processes could cause REE patterns to be more Ce-enriched and Dy_N/Sm_N decreased, which could be detected by negative correlation between Ce/Ce^* values and Dy_N/Sm_N ratios as well as positive correlation between Ce/Ce^* values and ΣREE concentrations. Both correlations are found in the phosphate fractions of the samples (Fig. 6c, d), especially the dolostone sub-samples, indicating alteration of Ce anomalies during the processes of phosphogenesis. On the contrary, rare correlations are displayed in the carbonate fractions between Ce/Ce^* values and Dy_N/Sm_N ratios as well as Ce/Ce^* values and ΣREE concentrations (Fig. 6c, e), indicating that they have not been obviously altered by diagenetic alteration.

Phosphate fractions from the phosphorite sub-samples show more variable Ce/Ce^* values and some are higher than those from the dolostone sub-samples, but an opposite trend is found in the carbonate fractions (Fig. 6f). This may be caused by REE enrichment in phosphorites during diagenetic processes. Regarding the different phosphorite layers, samples from the Lower Phosphorite Layer display weaker negative Ce anomalies compared to samples from the Upper Phosphorite Layer with moderate negative Ce anomalies, suggesting that the Lower Layer with thick phosphorite ores may have been affected by stronger diagenetic alterations.

In brief, all the parameters shown in Fig. 6 suggest that negative Ce anomalies preserved in the carbonate fractions of the samples could represent paleo-seawater redox environment during sedimentary processes. These samples, especially the dolostone sub-samples, display Ce/Ce^* values ranging from 0.44 to 0.72, indicating anoxic conditions in the ambient seawater during sedimentation. The negative Ce anomalies preserved in the phosphate fractions display higher Ce/Ce^* values, which can be regarded to represent redox conditions during diagenetic stages.

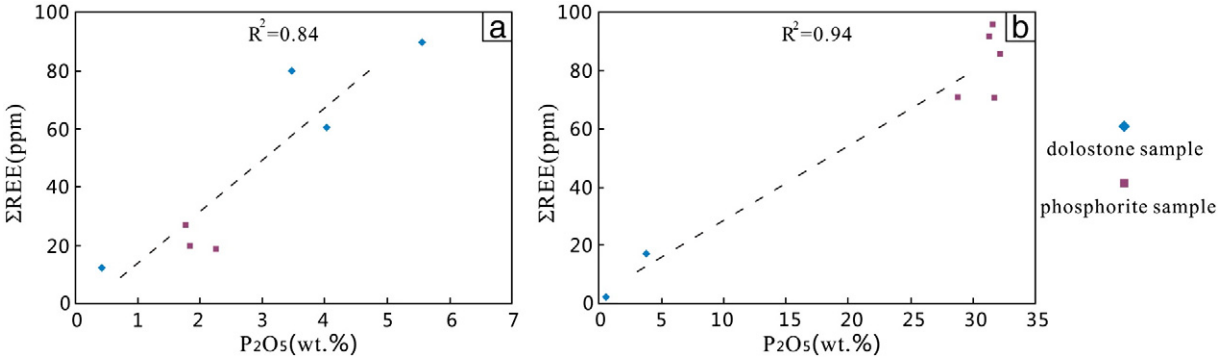

Fig. 5. Correlation between total rare earth elements (ΣREE) concentrations and P_2O_5 (wt.%) in bulk rock samples from the Zhangcunping section. (a) samples from the Upper Phosphorite Layer; (b) samples from the Lower Phosphorite Layer.

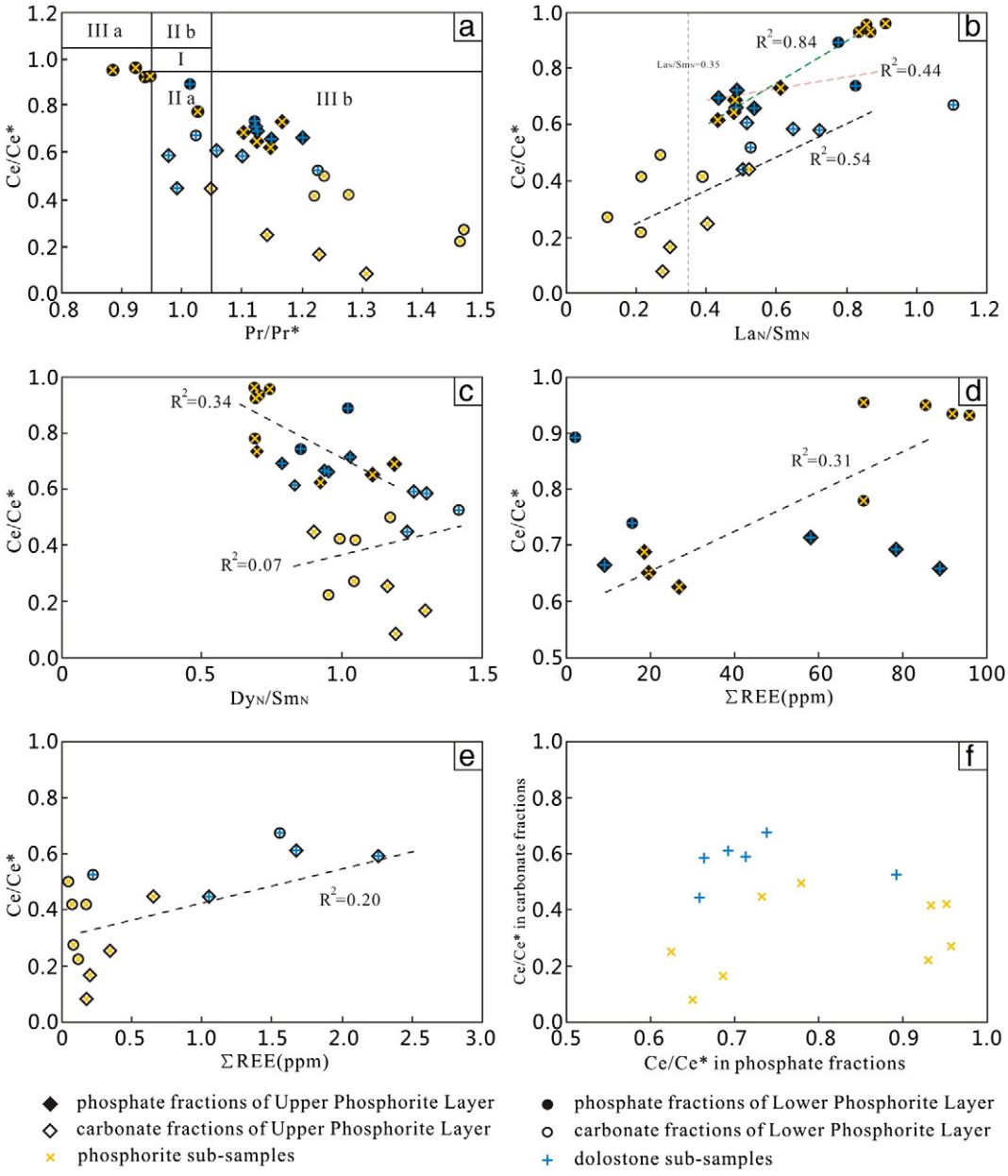

Fig. 6. Plots of Ce anomaly with various other REE parameters of different samples and fractions in the Zhangcunping section. Plot (a) evaluates whether Ce anomalies are overestimated by La enrichments, and in this plot, Filed I: no La and Ce anomaly; IIa: positive La anomaly and no Ce anomaly; IIb: negative La anomaly and no Ce anomaly; IIIa: positive Ce anomaly; IIIb: negative Ce anomaly (After Bau and Dulski, 1996).

5.3. Eu anomaly

Eu anomaly is usually found because of different valences of Eu compared to strictly trivalent valence of the other REEs (De Baar et al., 1985). Positive Eu anomalies have already been reported for phosphorites in different geological period and are believed to indicate reducing or anoxic conditions (Jiang et al., 2007; Kidder et al., 2003; Ogihara, 1999; Zhu et al., 2014). Redox shifts between Eu(II) and Eu(III) occur at high temperatures, and therefore Eu/Eu* signatures may retain source terrain redox environment. Eu^{2+} exists as the common form under reducing conditions, moving into the phosphates and producing positive Eu anomalies. Except the reducing environment, submarine hydrothermal fluid could also cause positive Eu anomaly (Jiang et al., 2007; Michard et al., 1983; Pi et al., 2013; Stalder and Rozendaal, 2004).

In our study the phosphate fractions of the samples display slightly positive Eu anomalies with Eu/Eu* ratios ranging from 1.01 to 1.32, while the carbonate ones show a larger variation from 1.06 to 37.46. However, because of the interference of Ba to Eu during ICP-MS measurement (Dulski, 1994), data of Eu as well as Eu anomalies can be affected due to high Ba concentrations. This can be detected by existence of positive correlation between Eu/Eu* values and Ba/Sm (Jiang et al., 2007) or Ba/Nd ratios (Ling et al., 2013). As shown in Fig. 7, Eu anomalies displayed in the carbonate fractions show fairly good positive correlations with Ba/Nd ratios (Fig. 7b) so that Eu anomalies in these samples will not be used for further discussion. However, Eu anomalies displayed in the phosphate fractions show less correlations with Ba/Nd ratios (Fig. 7a), especially in the samples with low Ba concentrations, indicating that these Eu anomalies are the real ones and can be used as the genetic indicators.

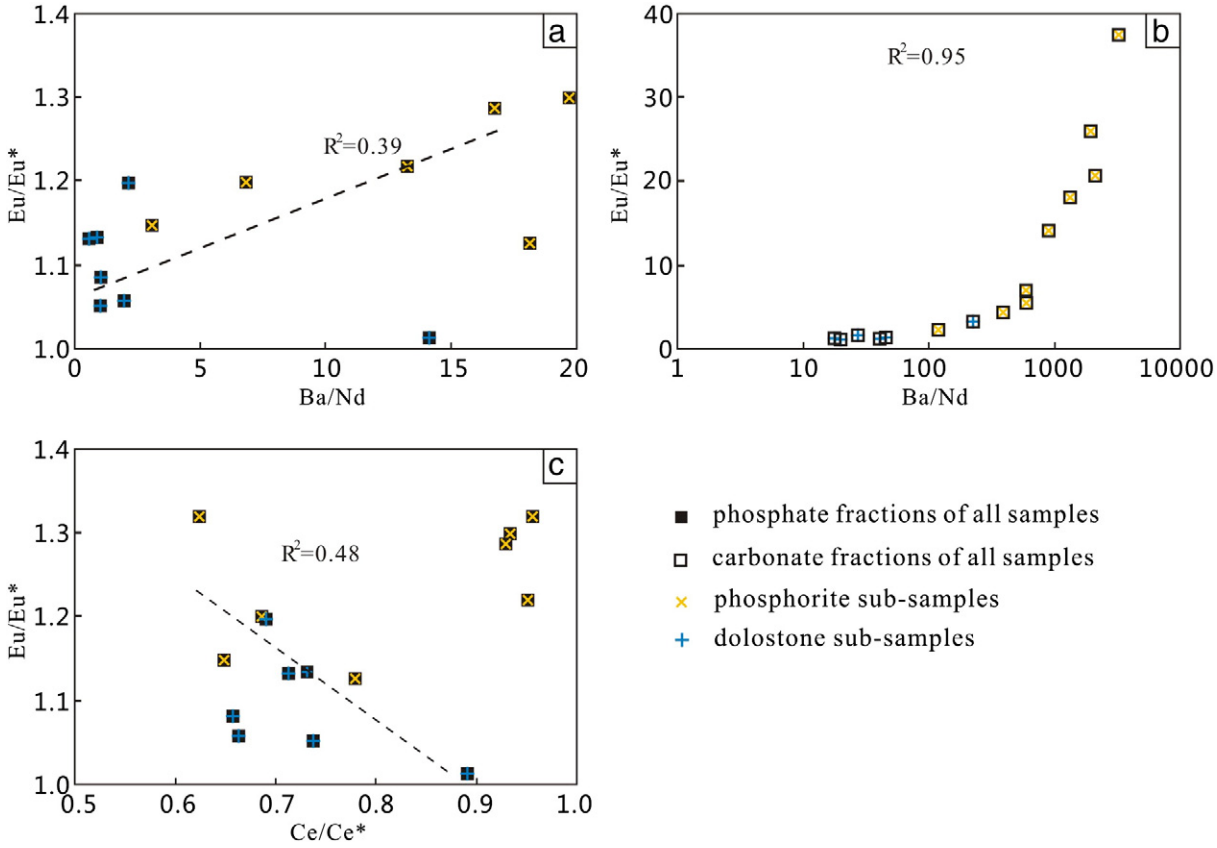

Fig. 7. Plots of Eu anomaly with various other REE parameters of different samples and fractions in the Zhangcunping section.

These valid Eu anomalies are displayed mainly in the dolostone sub-samples with Eu/Eu^* values from 1.01 to 1.32. As the lack of evidence to hydrothermal origin in our study area, we suggest that positive Eu anomalies should be caused by redox conditions. In reducing and anoxic conditions, Eu^{2+} can be reduced from Eu^{3+} and easily replace Ca^{2+} in apatite lattice so that the degree of Eu anomaly could indicate the paleo-environments (Jiang et al., 2007). As mentioned before, the phosphate fractions can only represent redox conditions of the diagenetic stages, which should be anoxic environments based on Ce anomalies. The negative correlation between the Eu/Eu^* and Ce/Ce^* values (Fig. 7c) indicates the coherence of redox conditions as decreased in Ce anomaly and Eu-depleted caused by diagenetic processes (Shields and Stille, 2001).

5.4. Nd–Sr isotopes

We have no data for the carbonate fractions of the samples due to the extremely low REE concentrations (Table 2). The εNd(t) values in the phosphate fractions of the samples vary from −6.9 to −3.8, and the phosphorite sub-samples and dolostone sub-samples show different ranges of −6.9 to −6.0 and −5.5 to −3.8, respectively. Yang et al. (1997) reported εNd(t) values of −7.0 to −5.1 of seven Ediacaran phosphorite samples from South China, which are coincident with the results in this study. All these values are in the range of modern seawater (−14 to 0) (Pieogras and Wasserburg, 1980). The negative εNd(t) values demonstrate that continental crustal sources should be the dominate REE source of seawater, which may be transported into to the ocean by river as a result of continental weathering (Yang et al., 1997). As the incorporation of Nd is nearly completed during early diagenesis (Martin and Scher, 2004), the εNd(t) values remain the primary surrounding water characteristics and the variations indicate changes of pore water Nd isotopic compositions during the formation of phosphorites. Furthermore, negative correlation between Nd content and εNd(t) shown in Fig. 8a indicates that εNd(t) decreases with the enrichment of Nd. Higher εNd(t) values are found in samples from the Upper Phosphorite Layer, whereas samples from the Lower Phosphorite Layer tend to display more negative εNd(t) values. In this case we can infer that εNd(t) values should be the results of mixing of seawater with higher εNd(t) value and diagenetic fluids with possibly lower εNd(t) value, while the Lower Phosphosrite Layer shows greater diagenetic effect. This inference agrees well with the explanation based on variations in REE patterns and Ce anomalies as we discussed above. At earlier stage of diagenesis, seawater was the dominated factor of pore water compositions. With the increase of burial depth, diagenetic fluids with lower εNd(t) controlled pore water composition gradually and overprinted seawater features finally. In addition, the negative correlation between εNd(t) values and initial $^{87}Sr/^{86}Sr$ ratios (Fig. 8b) also supports this explanation.

The initial $^{87}Sr/^{86}Sr$ ratios of the phosphate and carbonate fractions in the samples range from 0.709876 to 0.716797 and 0.708504 to 0.718641, respectively. Most samples have much higher initial $^{87}Sr/^{86}Sr$ ratios than the Ediacaran seawater (0.7075–0.7090) and present seawater (0.7092) (Halverson et al., 2010; Jacobsen and Kaufman, 1999; Li et al., 2012) except for some dolostone ones (0.708504–0.709958). These ratios varying from 0.7080 to 0.7100 are coincident with the former studies. As Sr isotopes are changeable during diagenetic processes (e.g. Hein et al., 1993; Rao et al., 2008; Stille et al., 1994), the $^{87}Sr/^{86}Sr$ ratio differences between the samples and paleo-seawater as well as the samples from different phosphorite layers could be explained by diagenetic effects. Martin and Scher (2004) also pointed out that the Sr isotopes in fossil teeth can continue to change with the surroundings during burial and diagenesis. Besides, the positive correlation between initial $^{87}Sr/^{86}Sr$ ratios from the phosphate and carbonate fractions (Fig. 8c) shows little fractionation in different parts of the same sample.

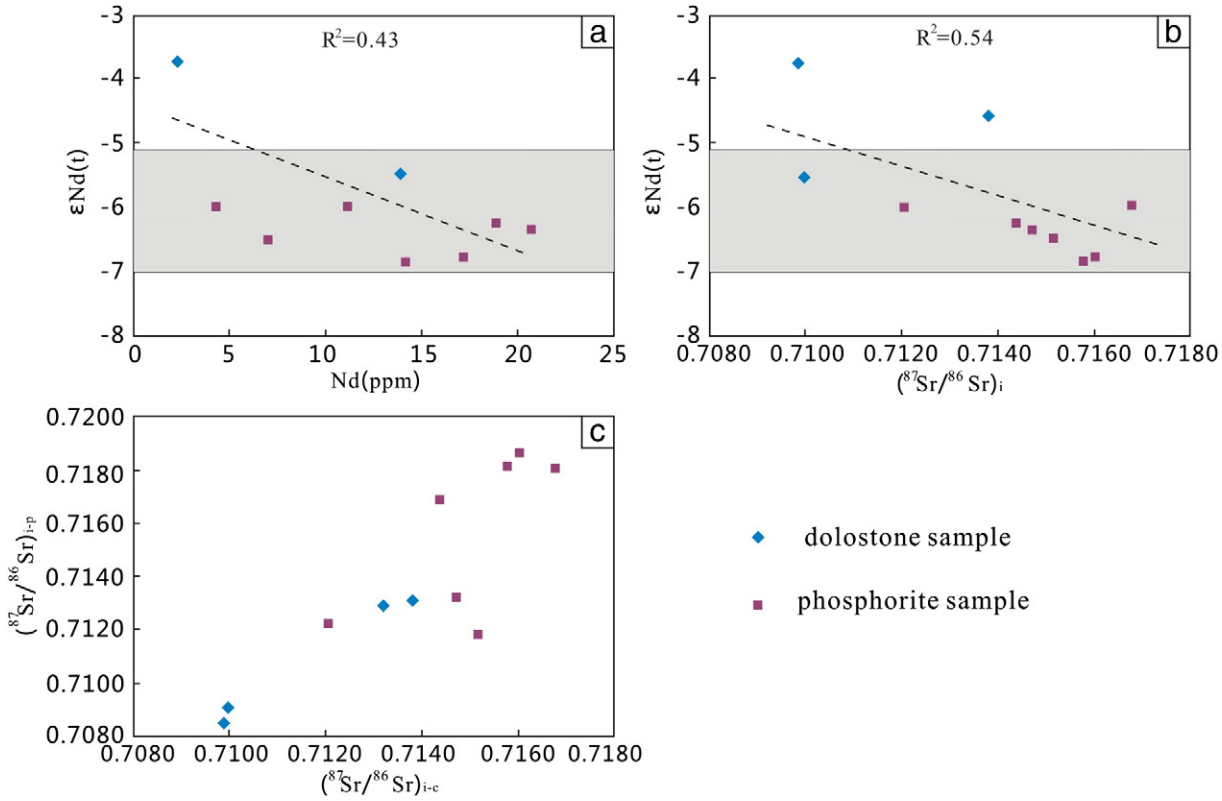

Fig. 8. Plots of Nd and Sr isotopic data of the Zhangcunping section samples. The shaded areas show the range of εNd(t) reported by Yang et al. (1997).

5.5. Phosphorite origin and REE sources

Marine phosphorite deposits always occur along the continental margins (Burnett, 1977) and the supply of phosphate in pore water is the prerequisite for ore formation (Trappe, 1998). The bacterial decomposition of organic material and reduction of absorbed phosphate on the surface of Fe-oxides are the two possible mechanisms of phosphate enrichment in pore water under anoxic conditions (Hesse and Schacht, 2011). Zhu et al. (2014) summarized different models for phosphorite genesis of early Cambrian in South China. As the stratified ocean was assumed to be widely developed during Neoproterozoic to early Cambrian period (Mazumdar et al., 1999), these models should be practical in our studied area. Shields and Stille (2001) and Trappe (1998) suggested that the ocean stratification and low sedimentation rate under anoxic bottom seawater conditions could result in the best preservation of organic matters. Jiang et al. (2007) proposed that the release of phosphate from Fe-oxides while deep water upwelling may be responsible for the precipitation of phosphorites.

There are many possible sources for REE in the phosphorites, such as seawater, ferromanganese oxide, organic matter and detrital silicate minerals (McArthur and Walsh, 1984; Trappe, 1998). In our study, the seawater-like REE patterns in the carbonate fractions indicate a seawater REE source. However, the carbonate ones supply much less REEs to the total rocks compared to the phosphate fractions, which display the hat-shaped REE patterns and indicate the detrital siliciclastic REE source dominantly. These two different sources can be distinguished by Y/Ho ratios: values of ~25–30 are characteristic of detrital siliciclastic sources of REEs, and values up to ~60 are characteristic of seawater sources of REEs (Bau and Dulski, 1996; Chen et al., 2015; Nothdurft et al., 2004; Webb and Kamber, 2000; Zhao et al., 2013). The Y/Ho ratios in phosphate fractions from all samples range from 25.50 to 46.07 (average value = 34.38 and SD = 5.95), which imply dominantly siliciclasitc sources of REEs as well as typical diagenetic influence. Meanwhile, the Y/Ho ratios in carbonate fractions range from 25.43 to 49.74 (average value = 36.71 and SD = 6.10), and the ones from Upper Phosphorite Layer range from 35.66 to 49.74 (average value = 41.05 and SD = 4.01), indicating mixing REE sources from siliciclastic and seawater as well as the less degree of diagenetic effect. The dominate REE source of detrital siliciclastic demonstrated by Y/Ho ratios is consistent with the conclusion by negative εNd(t) values.

Besides, Pi et al. (2013) considered the organic material as the dominating REE source for the kerogen in early Cambrian phosphorites. Felitsyn and Morad (2002) also found the same mechanism in Neoproterozoic phosphorite and they also considered organic matter as the supplier for both phosphate and REE. Moreover, the two types of REE patterns displayed are similar to those of some fossil organisms (Wright et al., 1984, 1987).

6. Conclusions

1) The phosphatic rocks from the Zhangcunping section in Neoproterozoic Ediacaran Doushantuo Formation in South China show two different types of REE patterns, i.e., the seawater-like REE patterns and the hat-shaped REE patterns, the former corresponding to the carbonate fractions and the latter refers to the phosphate fractions. The differences may indicate changes of pore water geochemical characteristics during diagenesis. The carbonate fractions may preserve the ambient seawater characteristics, but the phosphate fractions indicate domination of diagenetic fluids with containing high ΣREE concentrations in pore water.

2) Negative Ce anomalies and positive Eu anomalies displayed in the carbonate fractions of phosphatic rock samples are suggested to record redox conditions of paleo-seawater authentically. The anoxic environment was well developed during the formation of phosphorites.

3) Detrital siliciclastic minerals should be the main REE source based on Y/Ho ratios and Nd isotopic values. Organic material would also be a possible source of REE.

Acknowledgment

This study is financially supported by the Key project of National Natural Science Foundation of China (Grant Nos. 41230102 and 41273009) and the National 973 project (Grant No. 2013CB835000). We thank Tao Yang, Wei Pu, Qian Liu and Haizhen Wei for their help with the geochemical and isotopic analyses. Prof. Thomas Algeo provided valuable comments and suggestions which improved the manuscript significantly.

References

Anderson, L.D., Delaney, M.L., Faul, K.L., 2001. Carbon to phosphorus ratios in sediments: implications for nutrient cycling. Glob. Biogeochem. Cycles 15 (1), 65–79.
Bau, M., Dulski, P., 1996. Distribution of yttrium and rare-earth elements in the Penge and Kuruman Iron-Formations, Transvaal Supergroup South Africa. Precambrian Res. 79, 37–55.
Burnett, W.C., 1977. Geochemistry and origin of phosphorite deposits from off Peru and Chile. Geol. Soc. Am. Bull. 88, 813–823.
Chen, J., Algeo, T.J., Zhao, L., Chen, Z.Q., Cao, L., Zhang, L., Li, Y., 2015. Diagenetic uptake of rare earth elements by bioapatite, with an example from Lower Triassic conodonts of South China. Earth-Sci. Rev. http://dx.doi.org/10.1016/j.earscirev.2015.01.013.
Condon, D., Zhu, M., Bowring, S., Wang, W., Yang, A., Jin, Y., 2005. U–Pb ages from the neoproterozoic Doushantuo Formation, China. Science 308, 95–98.
De Baar, H.J.W., Bacon, M.P., Brewer, P.G., 1985. Rare earth elements in Pacific and Atlantic Oceans. Geochim. Cosmochim. Acta 49, 1943–1959.
De Baar, H.J.W., Schijf, J., Byrne, R.H., 1991. Solution chemistry of the rare-earth elements in seawater. Eur. J. Solid State Inorg. Chem. 28 (S), 357–373.
Dulski, P., 1994. Interferences of oxide, hydroxide and chloride analyte species in the determination of rare-earth elements in geological samples by inductively-coupled plasma-mass spectrometry. Fresenius J. Anal. Chem. 350, 194–203.
Felitsyn, S., Morad, S., 2002. REE patterns in latest Neoproterozoic–early Cambrian phosphate concretions and associated organic matter. Chem. Geol. 187, 257–265.
German, C.R., Elderfield, H., 1990. Application of the Ce anomaly as a paleoredox indicator: the ground rules. Paleoceanography 5, 823–833.
Gnandi, K., Tobschall, H.J., 2003. Distribution patterns of rare-earth elements and uranium in tertiary sedimentary phosphorites of Hahotoé–Kpogamé, Togo. J. Afr. Earth Sci. 37, 1–10.
Guo, Q.J., Shields, G., Liu, C.Q., Strauss, H., Zhu, M.Y., Pi, D.H., Goldberg, T., Yang, X.L., 2007. Trace element chemostratigraphy of two Ediacaran–Cambrian successions in South China: implications for organosedimentary metal enrichment and silicification in the early Cambrian. Palaeogeogr. Palaeoclimatol. Palaeoecol. 254, 194–216.
Halverson, G.P., Wade, B.P., Hurtgen, M.T., Barovich, K.M., 2010. Neoproterozoic chemostratigraphy. Precambrian Res. 182, 337–350.
Hein, J.R., Yeh, H.W., Gunn, S.H., Sliter, W.V., Benninger, L.M., Wang, C.H., 1993. Two major Cenozoic episodes of phosphogenesis recorded in equatorial Pacific seamount deposits. Paleoceanography 8, 293–311.
Hesse, R., Schacht, U., 2011. Chapter 9—early diagenesis of deep-sea sediments. Dev. Sedimentol. 63, 557–713.
Ilyin, A.V., 1998. Rare-earth geochemistry of 'old' phosphorites and probability of syngenetic precipitation and accumulation of phosphate. Chem. Geol. 144, 243–256.
Jacobsen, S.B., Kaufman, A.J., 1999. The Sr, C and O isotopic evolution of Neoproterozoic seawater. Chem. Geol. 161, 37–57.
Jarvis, I., Burnett, W., Nathan, Y., Almbaydin, F., Attia, A., Castro, L., Flicoteaux, R., Hilmy, M.E., Husain, V., Qutawnah, A., 1994. Phosphorite geochemistry: state-of-the-art and environmental concerns. Eclogae Geol. Helv. 87, 643–700.
Jiang, S.Y., Zhao, H.X., Chen, Y.Q., Yang, T., Yang, J.H., Ling, H.F., 2007. Trace and rare earth element geochemistry of phosphate nodules from the lower Cambrian black shale sequence in the Mufu Mountain of Nanjing, Jiangsu Province, China. Chem. Geol. 244, 584–604.
Kidder, D., Krishnaswamy, R., Mapes, R.H., 2003. Elemental mobility in phosphatic shales during concretion growth and implication for provenance analysis. Chem. Geol. 198, 335–353.
Li, C., Chen, J., Hua, T., 1998. Precambrian sponges with cellular structures. Science 279, 879–882.
Li, D., Ling, H.F., Shields-Zhou, G.A., Chen, X., Cremonese, L., Och, L., Thirlwall, M., Manning, C.J., 2012. Carbon and strontium isotope evolution of seawater across the Ediacaran–Cambrian transition: evidence from the Xiaotan section, NE Yunnan, South China. Precambrian Res. 225, 128–147.
Ling, H.F., Chen, X., Li, D., Wang, D., Shields-Zhou, G.A., Zhu, M.Y., 2013. Cerium anomaly variations in Ediacaran–earliest Cambrian carbonates from the Yangtze Gorges area, South China: implications for oxygenation of coeval shallow seawater. Precambrian Res. 225, 110–127.
Liu, P., Yin, C., Gao, L., Tang, F., Chen, S., 2009. New material of microfossils from the Ediacaran Doushantuo Formation in the Zhangcunping area, Yichang, Hubei Province and its zircon SHRIMP U–Pb age. Chin. Sci. Bull. 54 (6), 1058–1064.
Martin, E., Scher, H., 2004. Preservation of seawater Sr and Nd isotopes in fossil fish teeth: bad news and good news. Earth Planet. Sci. Lett. 220, 25–39.
Mazumdar, A., Banerjee, D.M., Schidlowski, M., Balaram, V., 1999. Rare-earth elements and Stable Isotope Geochemistry of early Cambrian chert-phosphorite assemblages from the Lower Tal Formation of the Krol Belt (Lesser Himalaya, India). Chem. Geol. 156, 275–297.
McArthur, J.M., Walsh, J.N., 1984. Rare-earth element geochemistry of phosphorites. Chem. Geol. 47, 191–220.
McLennan, S.M., 1989. Rare-earth elements in sedimentary-rocks—influence of provenance and sedimentary processes. Rev. Mineral. 21, 169–200.
Michard, A., Albarede, F., Michard, G., Minster, J.F., Charlou, J.L., 1983. Rare-earth elements and uranium in high-temperature solutions from East Pacific rise hydrothermal vent field (13°N). Nature 303, 795–797.
Moffett, J.W., 1990. Microbially mediated cerium oxidation in sea water. Nature 345, 421–423.
Morad, S., Al-Aasm, I., 1994. Conditions of formation and diagenetic evolution of Upper Proterozoic phosphate nodules from southern Sweden: evidence from petrology, mineral chemistry and isotopes. Sediment. Geol. 88, 267–282.
Morad, S., Felitsyn, S., 2001. Identification of primary Ce-anomaly signatures in fossil biogenic apatite: implication for the Cambrian oceanic anoxia and phosphogenesis. Sediment. Geol. 143, 259–264.
Muscente, A.D., Hawkins, A.D., Xiao, S., 2014. Fossil preservation through phosphatization and silicification in the Ediacaran Doushantuo Formation (South China): a comparative synthesis. Palaeogeogr. Palaeoclimatol. Palaeoecol. http://dx.doi.org/10.1016/j.palaeo.2014.10.013.
Nothdurft, L.D., Webb, G.E., Kamber, B.S., 2004. Rare earth element geochemistry of Late Devonian reefal carbonates, Canning Basin Western Australia: confirmation of a seawater REE proxy in ancient limestones. Geochim. Cosmochim. Acta 68, 263–283.
Ogihara, S., 1999. Geochemical characteristics of phosphorite and carbonate nodules from the Miocene Funakawa Formation, western margin of the Yokote Basin, northeast Japan. Sediment. Geol. 125, 69–82.
Paytan, A., McLaughlin, K., 2007. The oceanic phosphorus cycle. Chem. Rev. 107, 563–576.
Pi, D.H., Liu, C.Q., Shields-Zhou, Graham A., Jiang, S.Y., 2013. Trace and rare earth element geochemistry of black shale and kerogen in the early Cambrian Niutitang Formation in Guizhou province, South China: Constraints for redox environments and origin of metal enrichments. Precambrian Res. 225, 218–229.
Picard, S., Lécuyer, C., Barrat, J.A., Garcia, J.P., Dromart, G., Sheppard, S.M.F., 2002. Rare earth element contents of Jurassic fish and reptile teeth and their potential relation to seawater composition (Anglo-Paris Basin, France and England). Chem. Geol. 186, 1–16.
Pieogras, D.J., Wasserburg, G.J., 1980. Neodynium isotopic variations in seawater. Earth Planet. Sci. Lett. 50, 128–138.
Pu, W., Gao, J.F., Zhao, K.D., Ling, H.F., Jiang, S.Y., 2005. Separation method of Rb–Sr, Sm–Nd using DCTA and HIBA. J. Nanjing Univ. (Nat. Sci.) 41, 445–450.
Rao, V.P., Hegner, E., Naqvi, S.W.A., Kessarkar, P.M., Ahmad, S.M., Raju, D.S., 2008. Miocene phosphorites from the Murray Ridge, northwestern Arabian Sea. Palaeogeogr. Palaeoclimatol. Palaeoecol. 260, 347–358.
Rasmussen, B., Buick, R., Taylor, W.R., 1998. Removal of oceanic REE by authigenic precipitation of phosphatic minerals. Earth Planet. Sci. Lett. 164, 135–149.
Reynard, B., Lécuyer, C., Grandjean, P., 1999. Crystal-chemical controls on rare-earth element concentrations in fossil biogenic apatites and implications for paleoenvironmental reconstructions. Chem. Geol. 155, 233–241.
Sawaki, Y., Ohno, T., Tahata, M., Komiya, T., Hirata, T., Maruyama, S., Windley, B.F., Han, J., Shu, D., Li, Y., 2010. The Ediacaran radiogenic Sr isotope excursion in the Doushantuo Formation in the Three Gorges area, South China. Precambrian Res. 176 (1-4), 46–64.
Shields, G., Stille, P., 2001. Diagenetic constraints on the use of cerium anomalies as palaeoseawater redox proxies: an isotopic and REE study of Cambrian phosphorites. Chem. Geol. 175, 29–48.
Shields, G.A., Webb, G.E., 2004. Has the REE composition of seawater changed over geological time? Chem. Geol. 204, 103–107.
Stalder, M., Rozendaal, A., 2004. Apatite nodules as an indicator of depositional environment and ore genesis for the Mesoproterozoic Broken Hill-type Gamsberg Zn–Pb deposit, Namaqua Province, South Africa. Mineral. Deposita 39, 189–203.
Stille, P., Riggs, S., Clauer, N., Ames, D., Crowson, R., Snyder, S., 1994. Sr and Nd isotopic analysis of phosphorite sedimentation through one Miocene highfrequency depositional cycle on the North Carolina continental shelf. Mar. Geol. 117, 253–273.
Trappe, J., 1998. Phanerozoic phosphorite depositional systems. Lecture Notes in Earth Sciences 76. Springer, Berlin.
Wang, X.F., Erdtmann, B.D., Chen, X.H., Ma, X.D., 1998. Integrated sequence-, bio-and chemo-stratigraphy of the terminal Proterozoic to lowermost Cambrian black rock series from central South China. Episodes 21 (3), 178–189.
Webb, G.E., Kamber, B.S., 2000. Rare earth elements in Holocene reefal microbialites: a new shallow seawater proxy. Geochim. Cosmochim. Acta 64, 1557–1565.
Wright, J., Seymour, R.S., Shaw, H.F., 1984. REE and Nd isotopes in conodont apatite: variation with geological age and depositional environment. G. S. A. Spec. Pap. 196, 325–340.
Wright, J., Schrader, H., Holser, W.T., 1987. Paleoredox variations in ancient oceans recorded by rare earth elements in fossil apatite. Geochim. Cosmochim. Acta 51, 631–644.
Xiao, S., Zhang, Y., Knoll, A.H., 1998. Three-dimensional preservation of algae and animal embryos in a Neoproterozoic phosphorite. Nature 391, 553–558.
Xiao, S., Yuan, X., Steiner, M., Knoll, A.H., 2002. Macroscopic carbonaceous compressions in a terminal Proterozoic shale: a systematic reassessment of the Miaohe Biota, South China. J. Paleontol. 76, 347–376.

Yang, L., 2009. Accurate and precise determination of isotopic ratios by MC-ICP-MS: a review. Mass Spectrom. Rev. 28, 990–1011.
Yang, J.D., Tao, X.C., Xue, Y.S., 1997. Nd isotopic variations of Chinese seawater during Neoproterozoic through Cambrian. Chem. Geol. 135, 127–137.
Yin, L., Zhu, M., Knoll, A.H., Yuan, X., Zhang, J., Hu, J., 2007. Doushantuo embryos preserved inside diapause egg cysts. Nature 446, 661–663.
Yuan, X., Chen, Z., Xiao, S., Zhou, C., Hua, H., 2011. An early Ediacaran assemblage of macroscopic and morphologically differentiated eukaryotes. Nature 470, 390–393.
Zhao, L.S., Chen, Z.Q., Algeo, T.J., Chen, J., Chen, Y., Tong, J., Gao, S., Zhou, L., Hu, Z., Liu, Y., 2013. Rare-earth element patterns in conodont albid crowns: evidence for massive inputs of volcanic ash during the latest Permian biocrisis? Glob. Planet. Chang. 105, 135–151.
Zhou, C., Xie, G., Xiao, S., 2005. New data of microfossils from Doushantuo Formation at Zhangcunping in Yichang, Hubei province (in Chinese with English abstract). Acta Microbiol. Sin. 22 (3), 217–224.
Zhu, M.Y., Zhang, J.M., Steiner, M., Yang, A.H., Li, G.X., Erdtmann, B.D., 2003. Sinian–Cambrian stratigraphic framework for shallow- to deep-water environments of the Yangtze Platform: an integrated approach. Prog. Nat. Sci. 13, 951–960.
Zhu, B., Becker, H., Jiang, S.Y., Pi, D.H., Fischer-Gödde, M., Yang, J.H., 2013a. Re–Os geochronology of black shales from the Neoproterozoic Doushantuo Formation, Yangtze platform, South China. Precambrian Res. 225, 69–76.
Zhu, M.Y., Lu, M., Zhang, J.M., Zhao, F.C., Li, G.X., Yang, A.H., Zhao, X., Zhao, M.J., 2013b. Carbon isotope chemostratigraphy and sedimentary facies evolution of the Ediacaran Doushantuo Formation in western Hubei, South China. Precambrian Res. 225, 7–28.
Zhu, B., Jiang, S.Y., Yang, J.H., Pi, D.H., Ling, H.F., Chen, Y.Q., 2014. Rare earth element and Sr–Nd isotope geochemistry of phosphate nodules from the lower Cambrian Niutitang Formation, NW Hunan Province, South China. Palaeogeogr. Palaeoclimatol. Palaeoecol. 398, 132–143.